Representation of river channels in large scale flood inundation models

Jeffrey Neal[1,2], Laurence Hawker[1], James Savage[2], Michael Durand[3], Paul Bates[1,2], Christopher Sampson[2]

[1] School of Geographical Sciences, University of Bristol, UK. BS8 1SS
[2] Fathom, Square Works, 17-18 Berkeley Square, Clifton, Bristol, UK. BS8 1HB
[3] School of Earth Sciences, Ohio State University, USA.

Corresponding author: Jeffrey Neal (j.neal@bristol.ac.uk)

Key Points:
- Flood models in data sparse areas must estimate river bathymetry
- Existing methods are prone to over prediction bias
- Channel estimation based on gradually varied flow theory is substantially more accurate

Abstract

Flood inundation modelling across large data sparse areas has been increasing in recent years, driven by a desire to provide hazard information for a wider range of locations. The sophistication of these models has steadily advanced over the past decade due to improvements in remote sensing and modelling capability. There are now several global flood models (GFMs) that seek to simulate water surface dynamics across all rivers and floodplains regardless of data scarcity. However, flood models in data sparse areas lack river bathymetry because this cannot be observed remotely, meaning that a variety of methods for approximating river bathymetry have been developed from uniform flow or downstream hydraulic geometry theory.

We argue that bathymetry estimation in these models should follow gradually varying flow theory to account for both uniform and nonuniform flows. We demonstrate that existing methods for bathymetry estimation in GFM's are only accurate for kinematic reaches and are unable to simulate unbiased water surface profiles for reaches with diffusive or shallow water wave properties. The use of gradually varied flow theory to estimate bathymetry in a GFM reduced water surface profile errors by 66% and eliminated bias due to backwater effects. For a large-scale test case in Mozambique this reduced flood extends by 40% and floodplain storage by 79% at the 1 in 5 year return period. The results have significant implications for the role floodplains play in attenuating river discharges because previous GFM's based on uniform flow theory will overstate the role of the floodplain.

1 Introduction

In recent decades inundation modelling has become an integral component of flood management activities by providing hazard and risk mapping data to decision makers (Merz et al., 2010). Fundamental to this success has been the development of modelling frameworks where detailed river and floodplain bathymetry is combined with flow predictions or observations to construct numerical models that can simulate inundation depth for various scenarios (e.g. return periods) (de Moel et al., 2009). Results from such models have without question been useful to risk managers and are recognised by both national and international disaster risk reduction policies (Priest et al., 2016; Van Alphen et al., 2009). However, the expertise needed to implement these modelling methods, their data requirements and overall cost means that most flood risk data have been generated in developed countries, leading to substantial inequalities in risk information and an inadequate understanding of risk for many localities.

Perhaps unsurprisingly, there has been a move towards extending flood predictions to data and resource sparse areas, and in some cases using automated modelling approaches to enable regional or global coverage (Dottori et al., 2016; Sampson et al., 2015; Ward et al., 2015; Winsemius et al., 2013). This has been supported by better numerical codes and improvements in the availability and accuracy of key datasets, such as global elevation models (Yamazaki et al., 2017) and river width data (Allen & Pavelsky, 2018). Examples of regional and global scale inundation modelling now cover a range of applications including flood hazard estimation (Alfieri et al., 2014; Pappenberger et al., 2012; Sampson et al., 2015; Winsemius et al., 2013), flood event set and loss estimates (Quinn et al., 2019), flood risk and exposure modelling (Jongman et al., 2012; Ward et al., 2013), discharge estimation from remote sensing (Andreadis et al., 2007; Biancamaria et al., 2011; Durand et al., 2008; Neal et al., 2009), understanding wetland dynamics (Neal et al., 2012), estimating climate change impacts on flooding (Alfieri et al., 2017; Dottori et al., 2018; Hirabayashi et al., 2013) and modelling evaporative feedback to the atmosphere from wetlands (Dadson et al., 2010).

Despite wide ranging applications, the accuracy of global flood model predictions is poorly understood, but also likely to be low in many cases given that different models tend to disagree on where is at risk (Bernhofen et al., 2018; Trigg et al., 2016), and this is particularly the case over complex floodplains such as deltas. Furthermore, the models all over-predict exposure for more frequent events (smaller magnitudes) relative to loss observations (Quinn et al., 2019), which is often assumed to result from a lack of flood defence information (Ward et al., 2013). While not doubting the importance of flood defences, and there are noteworthy efforts to improve these data (Scussolini et al., 2016), it is imperative that the inundation model simulates an accurate water profile with respect to the river bank and floodplain heights. This is because most floodplains are inherently flat, and thus a small increase in simulated in-channel water height can generate a substantial increase in simulated flood extent. It follows that modest biases in the simulated water profile around bankfull discharge will adversely impact model accuracy during small high-frequency flood events. This has significant practical implications as high-frequency events must inherently make up the majority of events in any quantitative risk calculation (such as a loss-exceedance curve), and therefore they have the ability to significantly impact resultant risk estimates (e.g. Quinn et al., 2019).

This paper will review the methods used for river network definition when modelling floods in data sparse areas, focusing on their effectiveness at reproducing water surface profiles. Current methods are shown to be vulnerable to substantial errors when simulating river water surface

82 profiles under nonuniform flow conditions, which we demonstrate results in an over-prediction
83 of hazard. To address these issues and provide more robust simulation, improved approaches to
84 river channel definition in the absence of cross-section data are proposed based on gradually
85 varied flow theory. These approaches provide the necessary control over the behaviour of
86 channel-floodplain interaction in data sparse areas and lead to simulations that are more
87 consistent with the wave theories that underpin the inundation modelling.

1.1 Approaches to flood inundation modelling in data scarce areas

89 In the most basic terms, all flood inundation models require at least four components, with the
90 last item on this list being the focus of this paper:
91   1. Inputs that define the volumes of water flowing in the model domain
92   2. A numerical modelling approach to simulate river and floodplain flows
93   3. A definition of the floodplain surface over which the water might flow
94   4. A definition of the river network - specifically bank full conveyance and the subordinate
95   variables of channel width, depth, section shape and friction.

96 Each of these four components can be handled quite differently depending on the intended
97 application of the model, the balance needed between compute speed and accuracy, the data
98 available and the expertise of the model developers. For example, volume inputs can range from
99 direct observation of past events at gauges (Pappenberger et al., 2006), to design hydrographs
100 representing extreme events via a regionalization of gauging station data (Flood estimation
101 handbook, 1999; Smith et al., 2015), to runoff inputs from hydrological and land surface models
102 (Dottori et al., 2016; Winsemius et al., 2013; Yamazaki et al., 2011). The numerical
103 representation of river channel hydraulics in inundation models also varies substantially in
104 complexity, encompassing methods such as linear advection and diffusion wave methods
105 (Lohmann et al., 1998), kinematic waves (Bell et al., 2007; Oki & Sud, 1998), diffusive waves
106 (Sayama et al., 2012; Yamazaki et al., 2011), dynamic waves (diffusion + local inertia) (Neal et
107 al., 2012; Yamazaki et al., 2013) and shallow water wave processes (Paiva et al., 2011; Sanders
108 & Schubert, 2019). These generally increase in complexity and accuracy of process
109 representation in the above order, with simpler methods generally applicable in fewer physical
110 settings or used for large scale modelling.

111 To simulate floodplain inundation, the channel model must be linked to a model representing the
112 floodplain conditioned on suitable digital elevation data (Courty et al., 2019; Ettritch et al., 2018;
113 Hawker et al., 2018; Marks & Bates, 2000; Sanders, 2007; Sanders et al., 2005). Approaches to
114 represent floodplain inundation range in much the same way as those for the channel, from
115 relatively simple DEM filling type methods (Nardi et al., 2019; Winsemius et al., 2013), where
116 no dynamics are assumed, to extending 1D model cross-sections onto the floodplain (UNISDR,
117 2015), to models that dynamically link the channel to large floodplain storage areas (Decharme
118 et al., 2008; Paiva et al., 2011; Yamazaki et al., 2011) to models that simulate inundation
119 dynamics in two-dimensions (Neal et al., 2012; Sanders & Schubert, 2019; Sayama et al., 2012).
120 As with the channel models, complexity, cost and accuracy generally increase as you move down
121 this list, with simpler models easier to apply over large areas. The spatial resolution of the
122 simulations is usually governed by the resolution of the floodplain topography and a trade-off
123 between acceptable computational cost and the spatial precision required by the application.

124 Finally, the model will require a definition of the river channel network, which acts as a critical
125 control on how water moves through a landscape. In the case of fluvial flooding, the river

126 channel is usually the main conveyor of discharge and will interact with the floodplain in a
127 complex manner as water moves both from and to the channel, depending primarily on
128 topography and friction variability (Fewtrell et al., 2011; Knight & Shiono, 1996). Even in the
129 case of other types of flooding, such as pluvial and coastal, the role of channel conveyance can
130 be significant. How channels are represented in a data scare setting where bathymetry has not
131 been observed will therefore influence inundation simulations significantly (Neal et al., 2012;
132 Sampson et al., 2015; Yamazaki et al., 2011), particularly at low return periods where small
133 changes in river conveyance can have a disproportionately large impact on the simulated
134 flooding. For traditional reach scale hydrodynamic modelling, the quality of river bathymetry
135 data, often in the form of channel cross-sections or surfaces from sonar data, is key to accurate
136 simulation of the relationship between discharge and water level (Cook & Merwade, 2009).
137 However, since such data are unavailable in data scarce contexts an approximation must be used
138 that best represents the water surface elevation and discharge relationship given the available
139 data (Grimaldi et al., 2018).

2 Methods for defining river channels in data sparse flood inundation models

141 Several approaches have been proposed to simulating channel hydrodynamics in the absence of
142 cross-section data. We review and categorize these starting from the simplest case of removing
143 the channel component from the model entirely. Note that the methods cited also vary
144 considerably in their treatment of hydrology, choice numerical scheme and floodplain DEM, but
145 these will be secondary considerations here.

146 For this discussion we will take as a starting point that the profile of the river water surface can
147 be defined as a gradually varied flow:

$$\frac{\partial h}{\partial x} = \frac{(S_0 - S_f)}{1 - Fr^2} \tag{1}$$

149 where h is depth, x is distance downstream, Fr is the Froude number, S_0 is the bed slope and S_f
150 is the friction slope. If we also assume that the river channel is rectangular, and that friction is
151 represented by Manning's equation then the friction slope is found via:

$$S_f = n^2 \left(\frac{Q}{wh}\right)^2 \left(\frac{wh}{2h+w}\right)^{-4/3} \tag{2}$$

153 where n is Manning's roughness coefficient, w is the channel width and Q is discharge. The
154 Froude number of the channel Fr is then

$$Fr = \frac{Q}{w\sqrt{gh}} \tag{3}$$

156 where g is acceleration due to gravity. We argue that the inundation models need to accurately
157 estimate the water surface profile p for bank full discharge Q_{bf} along the river if the model is to
158 simulate flooding during events or for specific design discharges. The simulation of the flow
159 profile below bank full is not a priority in this case, justifying the commonly used simplification
160 to a rectangular channel. Obtaining an accurate flow profile from equation 1 will depend on
161 identifying the bed friction (n), bed elevation (z) from which bed slope (S_0) is defined, channel
162 width (w) and bankfull discharge (Q_{bf}) along the river network. Developers and researchers have
163 approached defining these in several ways as outlined below in order of increasing complexity.

164 i) The no channel method

The simplest approach to represent the river network is to estimate bank full discharge and then remove this from the event or design flood discharge of interest. This 'excess discharge' is then used by a series of reach scale models of the floodplain without a river channel. This is a popular method due to the simplicity of not needing to estimate w, n, or z and can yield sensible results over large areas (Alfieri et al., 2014; Bradbrook et al., 2005; Dottori et al., 2016). However, floodplain flow pathways are usually complex and dominated by the interaction between the floodplain and channel (Lewin & Ashworth, 2014; Trigg et al., 2012). Essentially fast-moving water in the channel interacting with slow moving water on the floodplain is needed to correctly simulate wave propagation during a flood. This approach is also particularly sensitive to the presence of objects or errors in the topography that impede the propagation of the flood wave downstream because the channel network would mitigate for these by allowing water to return to the channel and move on downstream at greater velocity. Over prediction as a result of mass blockage effects is therefore a concern (e.g. Neal et al., 2012) such that this approach works best for simulating short reaches using very accurate terrain data e.g. the UK extreme flood zone maps of Bradbrook et al. (2005). Over large and complex floodplains and deltas we expect the method to become inaccurate (Neal et al., 2012; Sampson et al., 2015).

ii) Empirical/Hydraulic geometry methods

An alternative to removing the channel is to estimate its dimensions empirically given observations from surveyed rivers using downstream hydraulic geometry theory, as demonstrated in the GFM of Yamazaki et al. (2013). Downstream hydraulic geometry theory aims to estimate how the width and depth of the channel are related to bank full discharge by a series of power laws (Leopold and Maddock, 1953). These parameters have been estimated empirically from field observations over many sites to allow prediction at locations without observations (Andreadis et al., 2013; Hey & Thorne, 1986). Once depth has been established, the bed elevation is typically calculated by subtracting depth from the river bank height all along the river network as defined in the DEM (with the aid of some processing along the channel to reduce DEM noise (Yamazaki et al., 2013; Yamazaki et al., 2019)). This method benefits from being simple to implement but there is little chance that the desired surface profile will be simulated at bank full discharge because, 1) the hydraulic geometry parameters are uncertain and difficult to regionalise, with substantial variability expected between rivers; 2) the friction value in the hydrodynamic model will need to be estimated because there is no direct link between the hydraulic geometry parameters and friction parameters; and 3) changes in profile slope are not accounted for, meaning the hydrodynamic model will simulate a different water surface elevations to those expected.

Given that width is readily observable from remote sensing platforms (Isikdogan et al., 2017; Lin et al., 2020; Yang et al., 2020) versions of this approach where the widths and other observable factors are used to help predict the bed elevation or bank full discharge have also been proposed (Gleason & Smith, 2014; Grimaldi et al., 2018). This approach has the advantage of not needing an estimate of bank full discharge, however when width is used to predict the depth a reach will shallow when the channel narrows and deepen when it widens if widths are not appropriately reach averaged, thus changing the conveyance in an unrealistic manner. This method was used by Neal et al. (2012) over a delta where the proportions of flow bifurcating down tributaries were unknown and strong evaporative feedback meant that mass was not conserved along reaches. However, the power law parameters and model friction were so uncertain that they needed to be estimated from water surface observations via a computationally expensive calibration process.

210 iii) Uniform flow theory – Manning's equation method

211 A simple way to calculate the channel bathymetry is to assume that a uniform channel exists over
212 long distances when calculating the depth such that uniform flow formula can be used. Under
213 this assumption the bed slope S_0 and friction slope S_f are assumed equal, and if the channel is
214 further assumed to be sufficiently wide that hydraulic radius (cross sectional area divided by
215 wetted perimeter) is equal to depth (cross sectional area divided by width) then the channel depth
216 h can be calculated analytically using Manning's equation from the local water surface slope S,
217 friction n, width w and discharge Q.

$$h = \left(\frac{nQ}{S^{1/2}w}\right)^{3/5} \tag{4}$$

218

219 Following the GFM described by Sampson et al. (2015) the channel bed is found by subtracting
220 depths from a smoothed bank high profile. This approach overcomes some of the limitations of
221 the hydraulic geometry method by accounting for the friction parameterization of the model (i.e.
222 the friction might not be known but at least the same value can be used for the flood model and
223 bathymetry estimation) and allowing depth and width to vary inversely for the same bank full
224 discharge. However, we know that many controls exist on flows that cause the river to depart
225 from uniform conditions, for example constrictions in channel width, changes in discharge (e.g. a
226 tributary joining), changes in bed slope and the presence of water bodies such as lakes.
227 Backwater effects from these controls will be significant in most lowland channels (Trigg et al.,
228 2009) meaning that the Sampson et al., 2015 GFM over-predicts the water surface profile in
229 many places because the flood inundation model (LISFLOOD-FP) will simulate nonuniform
230 flow profiles.

231 iv) Nonuniform flow

232 A more accurate method than those above would be to use a bed profile that simulates the
233 desired water surface profile given the gradually varied flow equations themselves, such that
234 nonuniform flow is accounted for. Unlike the uniform flow case there is no analytical solution,
235 however solving these equations is well established when river bathymetry is defined (Chaudhry,
236 2008). The calculation process involves starting from a control section where the water level is
237 also known and then integrating upstream in the case of subcritical flows or downstream in the
238 case of supercritical flows (Henderson, 1966). In the GFM case, the profile has been observed
239 rather than the bathymetry and the control section can be a lake, the ocean or river where
240 uniform flow is assumed. To estimate a channel for a nonuniform flow profile we must therefore
241 find the channel bathymetry that best approximates the observed profile given equation 1.

242 The next sections present two bed estimation methods targeted at two test cases. The first test
243 evaluates the principal of using nonuniform rather than uniform flow theory to estimate the
244 channel bed. It considers a reach scale situation where the water surface profile has been
245 observed at a specific time and the discharge is known. The purpose of this test is to compare
246 with observed bathymetry and assess the potential for improved accuracy at reach scale. The
247 second test demonstrates practical application to a GFM. For this test we implement the bed
248 estimation globally by simplifying the approach in test 1. The GVF based method is then
249 benchmarked against the Manning's equation method of Sampson et al. (2015) for a test case in
250 Mozambique and Malawi.

3 Implementation and testing of bed estimation for gradually varied flows

3.1 Test case 1: Reach scale bed estimation from water surface elevation

The data for this test case were obtained for a widely studied reach of the River Severn (UK) that flows from Worcester to Tewkesbury (Bates et al., 2006; García-Pintado et al., 2015; Neal et al., 2015; Schumann et al., 2009). An observed water surface profile was sampled at 10 m intervals from a 0.5 m resolution airborne LiDAR survey conducted by the Environment Agency on the 12th December 2014 (similar to the approach of Smart et al. (2009)). LiDAR water surface returns for this reach are expected to include vertical error of 5-15 cm, equivalent to another flat surfaces. River discharge at the time of the LiDAR acquisition was measured at the Saxons Lode gauging station, around the middle of the study reach (See Figure 1 for map). Flows were within bank and assumed to be without error for the purpose of this test given the high-quality ultrasonic gauging station installed at this site and its use for operation flood forecasting (Q error <10% given the flow conditions). The gauged discharge of 225.6 m^3s^{-1} was assumed to be constant along the 25 km reach and the average slope was 0.0001 m m^{-1}. Observations of the lowest bed elevation and water surface top width were obtained from cross section data provided by the Environment Agency. Manning's roughness coefficient was assumed to be 0.035 unless otherwise stated, which is physically reasonable for a reach like this with a gravel bed and cohesive banks. As flows in this reach are always subcritical, the GVF solver requires a water surface elevation and depth at the downstream boundary. These were estimated from the LiDAR observations of water surface elevation, slope and channel top width using Manning's equation.
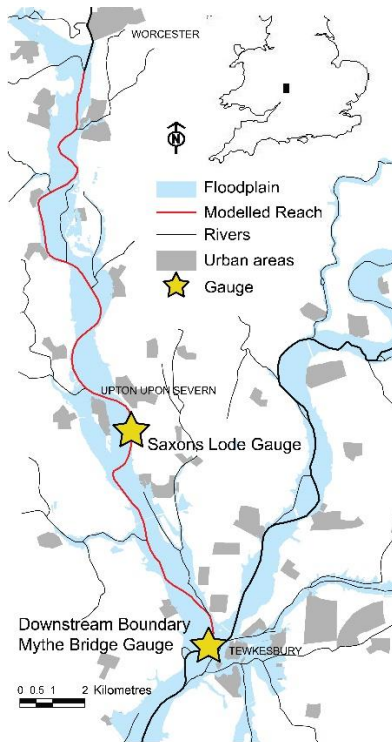

Figure 1. Map of River Severn test site including locations of gauging stations and downstream boundary conditions. The modelled reach is shown in red.

3.1.1 Estimating bathymetry

The bed estimation method presented below derives from recent work, in anticipation of the NASA Surface Water and Ocean Topography (SWOT) mission, which has focused on joint estimation of Q, n and z from a time series of water surface height and slope observations (Durand et al., 2016; Durand et al., 2014). Specifically, the method presented here is a simplification of that proposed by Garambois and Monnier (2015) for SWOT discharge and bathymetry estimation, which aimed aim to estimate Q, n and z from multiple observations of water surface elevation and slope through time. In our implementation Q and n will be known to the algorithm and there is no time element to our approach. Thus, our approach assumes discharge varies in space, but that the river can be approximated as steady state. This steady state assumption could be relaxed, at considerable computational expense, with the use of a 1D hydrodynamic model and time varying discharge in place of the gradually varied flow solver. Brêda et al. (2019) evaluate several data assimilation methods that would be suitable for bed estimation in such circumstances, thus these are not discussed here. Meanwhile there are a range of alternative methods for finding the inverse of the gradually varied flow equations or similar, which are reviewed in detail by Sellier (2016) but not tested here.

The steps taken to estimate the channel bed are outlined in Figure 2 and in detail below. A first-order estimate of the bed elevations are needed as initial conditions, which would most obviously come from the Manning's equation method (uniform flow assumption) described above. From these bed elevations the gradually varied flow profile given the Manning's method bed is found using the Runge-Kutta method to solve equation 1 (function ode45 in Matlab).

To refine the estimate of river bed elevations z from the first-order approximation, we seek the bed elevation that minimises the least squares difference between the desired water surface profile p and that simulated by the gradually varied flow solver. The response to changing bed elevation will be complicated due to backwater effects, therefore, nonlinear least squares optimization was undertaken using the trust region reflective method (More & Sorensen, 1983) to search within pre-defined bounds (z_{ub} and z_{lb}) for the bed elevation, where subscripts ub and lb signify the upper and lower bounds respectively. The optimisation function used here (lsqnonlin in Matlab) requires a vector of residual values (differences between observed and simulated profile) as input from which to compute the sum of square errors, therefore for the case where the water surface profile p is being estimated given discharge Q the following vector values are to be optimised

$$f(z) = M(z, Q, \theta) - p \ , \ z_{ub} > z > z_{lb} \tag{5}$$

Where θ contains all other parameters of the gradually varied flow solver e.g. roughness and channel widths and $M(z, Q, \theta)$ is the water surface elevation simulated by the gradually varied flow solver. This condition was enough to find a channel bed that simulates the desired water surface profile in this test. However, the solution is non-unique and in practical applications this method alone created undesirable outcomes in that the bed elevations varied from one estimation point to the next far more than expected. Essentially the magnitude of bed slopes is greater than expected and often includes substantial adverse slopes that are implausibly steep and inconsistent with natural bedforms. Therefore, we evaluate the effectiveness of including three additional costs to the objective function to regularise (simplify) the solution, which aim to reduce the variability in bed elevation from one location to the next by penalising for greater bed gradient (∇z), water surface gradient (∇z+h) or channel depth ($z_{bf} - z$). In other words, we are adding

318 regularisation terms to the optimisation to prefer simpler solutions that are shallow or give
319 gradually varying channel beds, or yield smooth water surfaces by passing one of the following
320 vectors to the optimiser:

321 $$f(\boldsymbol{z}) = \begin{bmatrix} M(\boldsymbol{z}, \boldsymbol{Q}, \boldsymbol{\theta}) - \boldsymbol{p} \\ \rho S^{-1} \nabla \boldsymbol{z} \end{bmatrix} \; ; \; f(\boldsymbol{z}) = \begin{bmatrix} M(\boldsymbol{z}, \boldsymbol{Q}, \boldsymbol{\theta}) - \boldsymbol{p} \\ \rho S^{-1} \nabla (\boldsymbol{z} + \boldsymbol{h}) \end{bmatrix} \; ; \; f(\boldsymbol{z}) = \begin{bmatrix} M(\boldsymbol{z}, \boldsymbol{Q}, \boldsymbol{\theta}) - \boldsymbol{p} \\ \rho (\boldsymbol{z}_{bf} - \boldsymbol{z}) \end{bmatrix} \quad \text{(6a, 6b, 6c)}$$

322 How much weight is given to each of the additional costs is determined by parameter ρ, where
323 the greater the parameter value the greater the weight and greater preference for a simple
324 solution to the bed. The weight given to the gradient based costs needs to vary depending on the
325 slope of a reach S to have a consistent effect against any given error magnitude. e.g. we expect
326 lower gradient rivers to require greater weights. Therefore, we normalise for this effect by
327 multiplying ρ by the river slope S in these cases. S can be estimated from the longitudinal water
328 surface, bank or floodplain elevations. In the next section we will test this this gradually varied
329 flow solver approach and examine the effect of ρ for cost functions in equations 6a-c on the
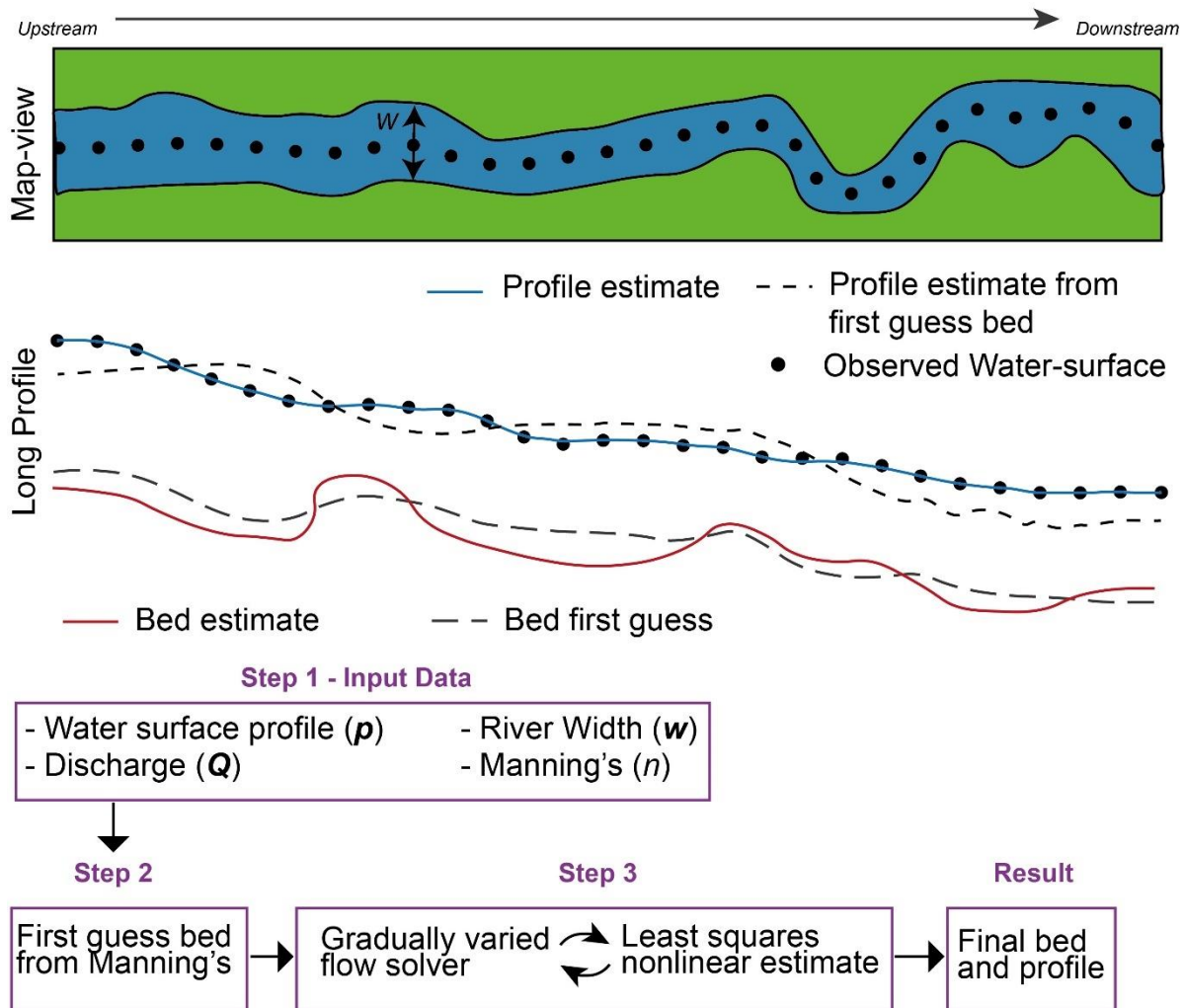330 optimization routine.

331

Figure 2. Conceptual diagram of a bed estimation method for test 1, using a gradually varied flow solver and non-linear least squares estimation approach.

3.1.2 Results from Test 1

A series of tests were implemented to assess different configurations of the bed solver objective function and establish the performance of the method verse assuming uniform flow. The simplest configuration seeks the minimum between the simulated water surface and the LiDAR water surface while the others give differing weights to the preference for a smooth and shallow bed and a smooth water surface as described by equations 6a-c. Upper and lower bounds for the bed (z_{ub} & z_{lb}) were set such that the channel could be no more than 30 m deep from the observed water surface and no higher than 5 m above the observed water surface. This range goes well beyond physically plausible values for depth for this reach which is typically in the range 6-8 m. Manning's equation was used to estimate the initial bed profile and to provide a benchmark. Details of the Manning's equation implementation are provided in the supplement, however when the Manning's bed profile was used as input to the gradually varied flow solver a root mean squared error (RMSE) of 0.34 m and mean error (ME) of -0.24 m to the LiDAR water surface was achieved.

Optimizing the bed elevation to the LiDAR water surface produced a water surface with a RMSE of 0.16 m and ME of 0.073 to the LiDAR observations, 53% more accurate and significantly less biased than the Manning's based approach. The bed profile is plotted in figure 3a and shows a high degree of bed variability relative to the observed data, with many locations where the channel is unrealistically deep relative to the observed bed.

The impacts of considering bed slope, water surface slope or bed depth in the cost function are plotted in figure 4, where (4a) plots RMSE against parameter ρ for each regularization term, (4b) plots the mean errors and (4c) plots the number of iterations the nonlinear least squares optimiser needed to find a solution (effectively the relative computational cost. The most accurate of the regularization terms preferred a lower gradient bed, which could reduce the RMSE to 0.095 m and the ME to -0.007 m for a ρ value of 0.046. This is a 72% reduction in RMSE relative to the Manning's model and is within the vertical error of the LiDAR survey. It is probably not desirable or possible to fit the observation data any better than this. Imposing a cost for deeper beds reduced the RMSE to 0.099 m with a mean error of 0.014 m for a slightly lower ρ value of 0.033, which at first glance suggests this regularisation approach could be almost as successful as the constraint on bed gradient. However, the range of ρ that produced good results (defined as results that are better than the approach without the regularisation) is much narrower and mean errors (over-prediction of the water surface) increase with the magnitude of ρ. Regularising on the water surface gradient could also reduce RMSE with higher values of ρ, however not by as much as the other two methods. This approach also required over twice the computational cost at the respective optimal values of ρ, suggesting it was better to regularise directly on the variable being estimated (channel bed elevations). Overall, the most accurate regularisation approach was to include a preference for a low gradient bed, which reduced water surface RMSE at no additional computational cost compared to not including the regularisation terms. Values for ρ >0 and <0.17 would all improve the simulation accuracy and bias, however an optimal value of 0.046 indicates that scaling the bed gradient to around half the observation errors in the water surface profile produced optimal results in this case. There might be benefits in combining the constraints, this is possible, and we did try it. However, RMSE was not improved with more

complex regularisation schemes, which was expected given the observation errors, while the inclusion of the shallow bed preference always increased the mean error due to the shallow bias. Further reach scale tests for a range of flow profiles would be needed to test the robustness of this conclusion.

Figures 3b-d plot bed estimates and corresponding simulated water surfaces for the shallow channel (3b) bed gradient (3c) and water surface gradient (3d) based regularisation approaches, all of which resulted in a simplification of the bed elevations relative to the no regularisation case in figure 3a, albeit the impact being minor in the case of the smooth water surface constraint. Therefore, the regularisation was successful in reducing the complexity of the riverbed profile and made it easier to find an optimal solution to the observed water surface. This result was expected given that the flow characteristics of this river are highly diffusive such that the water surface at any point reflects the integrated response to the downstream channel geometry, discharge and friction.

Finally, additional tests were conducted given channel friction values from 0.02 to 0.07, a range of initial starting depths from 1 m to 20 m, and a range of bed estimate and water surface observation resolutions from 100 m to 2,000 m. In all cases the smooth bed regularisation term ρ was set at 0.046 (the optimum from the previous experiments). The results of these experiments are tabulated in Table 1. Friction has a negligible impact on RMSE and ME, although lower friction values required more function calls to the GVF solver in order to perform the optimization, potentially because the channel is shallower and further from the first-order estimate based on Manning's equation. The initial bed elevation had no impact on RMSE or ME, demonstrating that the solver did not get stuck in local optima for this test. A better initial bed required substantially fewer function calls (around half) of a poor initial bed (e.g. 1 m or 20 m), but if Manning's equation is used for the initial bed and the friction is the same between the two method it is unlikely there will be many cases where the initial bed is as poor as some of those tested here. The resolution of the observations and bed estimation points influenced the accuracy of the results with respect to both RMSE and ME, with higher resolutions being more accurate as expected. For this reach, RMSE increased by a little over 0.02 m from 2 km to 1 km, but by only 0.1 cm from 1 km to 100 m. The number of function calls increased at finer resolution due to the need to estimate more bed elevations, between 2 km and 0.5 km the function calls per estimation point were essentially the same, but doubled for the 0.1 km resolution indicating that it was more difficult to fit finer resolution data.
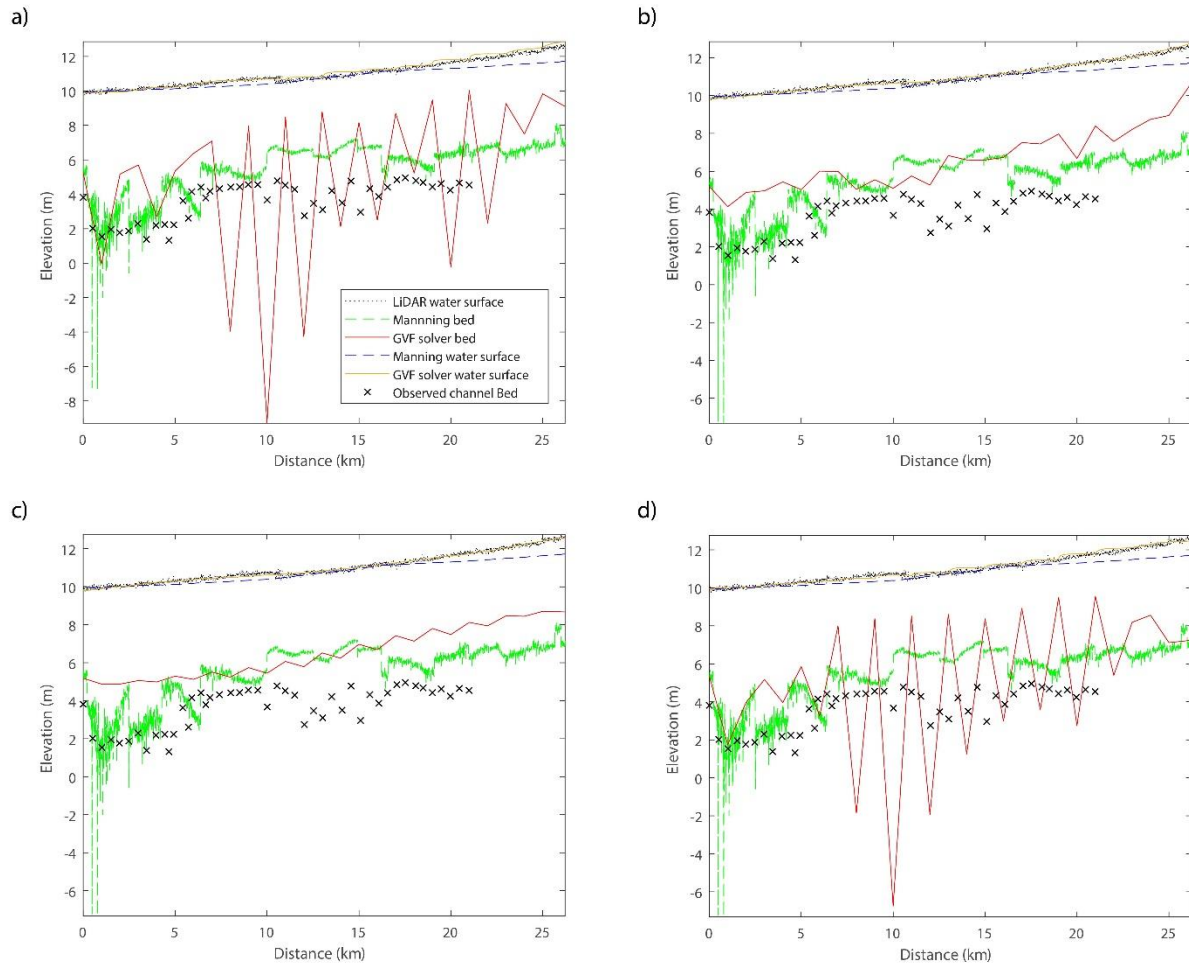
409

Figure 3. Optimised bed elevations and simulated water surfaces relative to LiDAR observations
for (a) GFV solver method with no regularisation terms, (b) GFV solver with shallow bed
preference, (c) GVF solver with low gradient bed preference, and (d) GVF solver with low
gradient water surface constraint. Also plotted is the initial bed estimated from Manning's
equation and the simulated water surface from this. Channel thalweg (lowest point of channel
bed) is also plotted where available, note that the assumption of a rectangular channel means we
would expect the optimal bed for the model to be above that of the real irregular river sections.
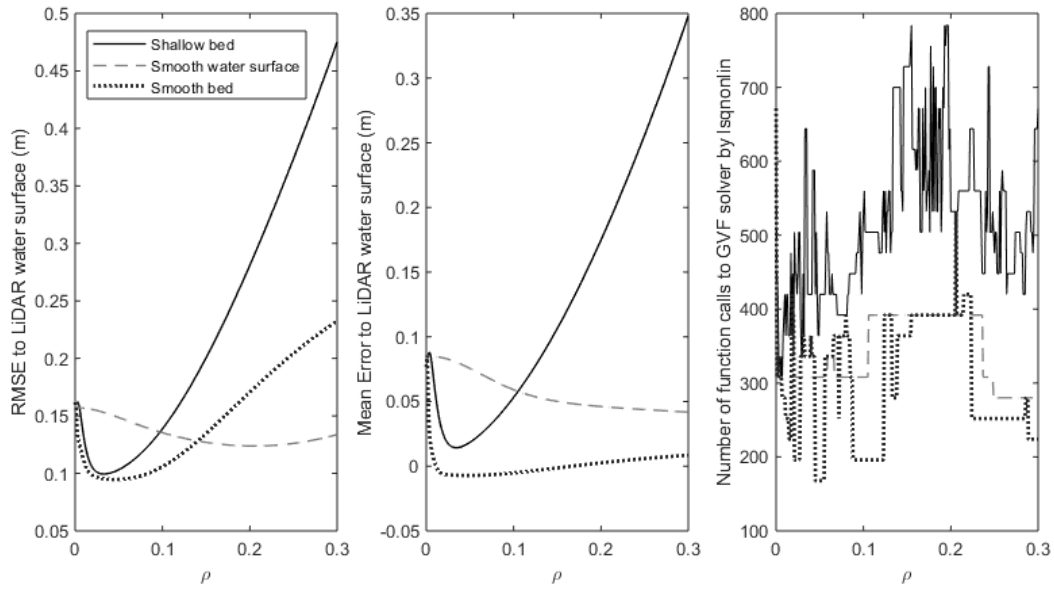
417

Figure 4. Performance of optimised channel beds for different cost functions and values of parameters ρ. Performance metrics are a) RMSE to LiDAR water surface, b) Mean Error to LiDAR water surface, & c) Number of function calls to the GFV solver by the nonlinear least squares estimation function.

Table 1. Impact of changing channel friction, initial depth of channel and resolution on GVF solver water surface accuracy (in terms of RMSE and ME to LiDAR water surface observations). Function calls to the GFV solver from the least squares nonlinear optimiser are also shown and are proportional to computation cost (note that the higher resolution models are also more expensive due to the number of estimation points).

Friction n	Initial bed	Resolution	RMSE	ME	Function calls
0.02	Manning	500 m	0.099	0.0025	336
0.03	Manning	500 m	0.095	-0.0055	336
0.04	Manning	500 m	0.094	-0.0085	168
0.05	Manning	500 m	0.094	-0.010	168
0.06	Manning	500 m	0.095	-0.010	168
0.07	Manning	500 m	0.095	-0.011	168
0.035	20 m deep	500 m	0.094	-0.007	336
0.035	10 m deep	500 m	0.094	-0.007	196
0.035	5 m deep	500 m	0.094	-0.007	168

0.035	2 m deep	500 m	0.094	-0.007	336
0.035	1 m deep	500 m	0.094	-0.007	392
0.035	Manning	2000 m	0.121	0.056	90
0.035	Manning	1000 m	0.094	-0.0073	168
0.035	Manning	500 m	0.094	0.0031	324
0.035	Manning	100 m	0.093	0.00029	3432

427

3.2 Test case 2: Implementation in a global flood model

429 Given the improved profile accuracy seen at the reach scale, a bed estimation method based on
430 gradually varied flow was implemented within a global flood model (GFM) (Sampson et al.,
431 2015; Wing et al., 2017). This model previously used the Manning's method for bed estimation
432 and is described in detail by Sampson et al. (2015). A full description of the GFM is beyond the
433 scope of this paper; however the key components include: i) a regional flood frequency analysis
434 (Smith et al., 2015) to provide return period discharge for all points on the global river network;
435 ii) river network and terrain data sets based on the MERIT DEM (Yamazaki et al., 2017) and
436 MERIT HYDRO (Yamazaki et al., 2019) from which river locations and floodplain elevations
437 were extracted; and iii) a regionalised river width estimation approach as described by Sampson
438 et al. (2015). Numerical simulations were performed using the LISFLOOD-FP hydrodynamic
439 model given the 1D channel from the bed solver and a 2D floodplain model based on MERIT
440 DEM. LISFLOOD-FP is a hydrodynamic model that solves a simplification of the shallow water
441 equation without convective acceleration terms (Bates et al., 2010; de Almeida et al., 2012). For
442 large scale applications, it uses a regular gird with either geographic (WGS84) coordinate
443 systems and a 1D sub-grid scheme for river channels (Neal et al., 2012; Sampson et al., 2015).
444 All rivers were assumed to convey the 1 in 2 year flow at bank full discharge; research elsewhere
445 is examining the sensitivity to this assumption.

446 The GFM was implemented at 3 arc second (~90 m resolution) with bed estimates linearly
447 interpolated from a 30 arc second (~900 m resolution) river network that includes all rivers with
448 an upstream catchment area above 50km^2. For small channels, the initial bank elevation profile p
449 was taken from DEM cells directly above the channel and conditioned using a local smoothing
450 function and monotonicity constraint. For larger rivers, a sample of elevation values for each
451 node was taken from DEM cells adjacent to the water mask to ensure that bank elevations (rather
452 than water elevations) were being sampled. A clustering algorithm was used segment the
453 sampled elevations, with the median value of the lowest cluster assumed to be the bank
454 elevation. As with small rivers, the channel elevation profile was then conditioned using a local
455 smoothing function and monotonicity constraint (Sampson et al., 2015). For global application
456 there are ~0.5 billion locations where the channel bed must be estimated. Thus, although it is in
457 theory possible to implement the GVF method as applied to the Severn test case globally,
458 computational constraints required a simplification to the estimation process whereby the trust
459 region reflective nonlinear least squares estimation was replaced by a simpler bed nudging

460 approach to optimise the bed elevations from the initial bed. This nudging involved the following
461 steps:

    462   i)   solve for the water surface profile given the initial bed estimate from Manning's
    463   equation,
    464   ii) compute the differences between bank profile and simulated water surface elevations
    465   from step 1,
    466   iii) apply the differences between the bank profile and simulated water surface from ii to the
    467   bed elevations,
    468   iv) recompute the water surface profile, and
    469   v) repeat ii, iii, iv once more to get a final set of bed elevation estimates and water surface
    470   profile errors.

471 The GFM is implemented as 10x10 degree overlapping tiles. Downstream boundary conditions
472 for each river were estimated using Manning's equation at the edge of each model tile or using
473 the GVF method results for the river mainstem where tributaries join. Coastal water heights were
474 set to mean sea level. For sections of supercritical flow, the channel depth was set to the critical
475 depth because the same Froude limit is applied in the LISFLOOD-FP inundation model when
476 implemented at large scale following Adams et al. (2017). A gradually varying flow solver
477 capable of simulating supercritical flow transitions could be used with shallow water
478 hydrodynamic models. A convenient implication of this assumption is that the GVF solver only
479 ever needs downstream boundary conditions as the supercritical profile is never simulated.

480 One GFM tile has been chosen here for further analysis to keep the data volume presentable in
481 the following plots. It covers 10°-20° south and 20°-30° east, which includes North and Central
482 Mozambique, Malawi, southern Tanzania and the eastern edges of Zambia and Zimbabwe.
483 Inundation data are presented for a smaller 3°x3° region including the town of Beira and the
484 mouth of the Zambezi river for visualisation purposes (Figure 5). Beira experienced substantial
485 flooding in 2019 due to cyclone Idai for which the GFM data were used to produce disaster
486 bulletins that include details of population exposure estimates (Emerton et al., 2020 (in review)).
487 Since the site includes the delta of the Zambezi, headwaters and extensive floodplains/wetlands
488 we believe it is indicative of most locations where GFM data may be used.
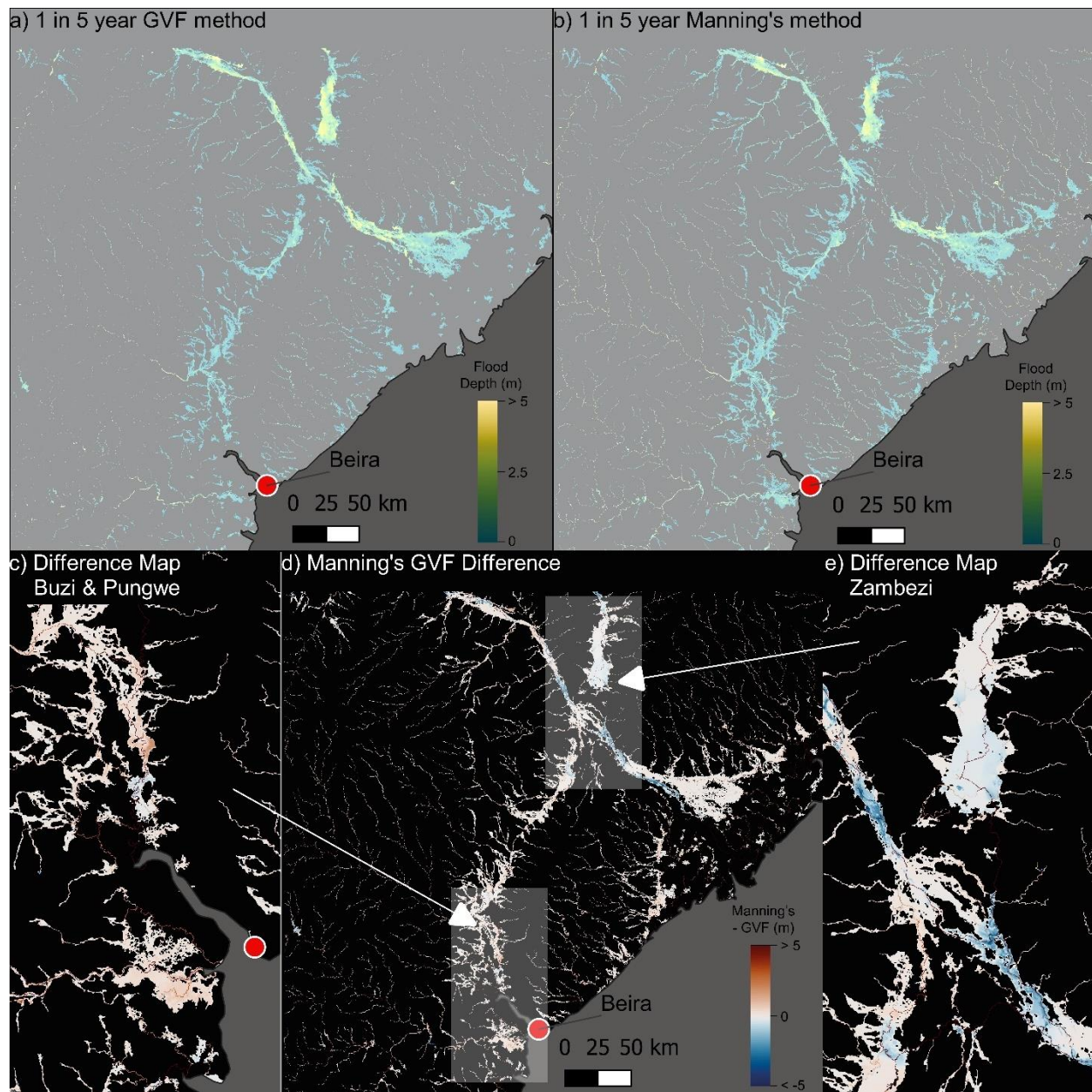
Figure 5. Flood inundation depths for the 1 in 5 year return period flows for the region around Beira and the mouth of the Zambezi River, Mozambique. Model run are identical except for the specification of bed elevations from a) Manning's method and b) GVF method.

Results from the Manning's and GVF method are presented in figure 6, which plots the difference between the water surface profiles at bank full discharge simulated by the two methods and bank height for all 144,523 channel locations within the domain. This accuracy measure is plotted against a) bank height, b) bankfull discharge, c) bank slope, and d) Froude number (defined by equation 3) in order to understand how the wave properties and physical setting affect water surface profile accuracy.

Overall, the root mean squared error between simulated water surface elevations and bank heights was 0.872 m for the Manning's method and 0.291 m for the GVF method. Mean error

was 0.167 m for the Manning's method and -0.030 m for the GVF method. From these numbers and visually in Figure 6 it was clear that the Manning's method tended to over predict the water surface relative to the target bank heights, whereas the grad solver was unbiased while also more accurate. Elevation and bank full discharge had no systematic impact on the magnitude of errors for either method. However, Manning's method errors were generally larger for slopes less than 10-3 m m^{-1}, with almost all of the overprediction at low Froude (<0.2). The GVF method was almost always more accurate than the Manning's method, however there were 16 points with Froude number >0.99 where errors exceed -2 m.– These points of poor performance correspond to steep features such as dam outlets and waterfalls, however the impact was limited locally to just a few model cells and did not propagate widely through the model domain. These errors are likely a weakness of out GVF solver setup in that we do not consider supercritical flow profiles or discontinuities.

Given the poor performance of the Manning's method at low Froude we investigated the relationship between water surface error and wave type following the approach of Trigg et al. (2009) following Vieira (1983). This was done by calculating the kinematic wave number k in addition to the Froude number at every river location:

$$k = \frac{S_0 L}{h Fr^2} \tag{7}$$

Where L is the channel length. When plotted against Froude number, suitable approximations for the wave at each point on the river network can be identified. According to the analysis of Vieira (1983), a kinematic wave is considered to be a reasonable approximation for locations with approximately $k > 10$ and $Fr > 0.5$, for $k > 3$ and $Fr < 0.5$ the wave can be characterised as diffusive, while shallow water characteristics are important for lower values of k. Figure 7 plots each river location into this wave characteristics space for both bed estimation methods. The dot colour indicates the magnitude of the profile error (truncated at 1 m to aid visualisation). Manning's method results (figure 7a) were only accurate for reaches that can be approximated by a kinematic wave, which was expected because uniform flow is assumed. The channel depth was underestimated where diffusive or shallow water wave processes become important. The poor performance of kinematic wave models over large lowland rivers and the important role backwater effects can have on flooding is well established (Ikeuchi et al., 2015; Trigg et al., 2009; Yamazaki et al., 2011) and these results are in line with the expectation that the Manning's bed estimation method would over-predict the water surface and flood extent.

The GVF method was more accurate when diffusive and shallow water wave characteristics were important, with errors >1 m mainly present at the very lowest Froude and kinematic wave numbers. Further investigation revealed these locations to be lakes (predominantly lake Malawi). It is important to note that the GFM does not include a bespoke routine for simulating lake levels. Rather, lakes are represented as very flat rivers with widths as defined as if they were rivers (Sampson et al., 2015). Given this combination of unrealistic lake widths and a flat bank it was not possible to accurately simulate the lake surface profile, and in classic applications of GVF theory lakes would usually form boundary conditions rather than be estimated. Furthermore, tributaries joining the lake connect to the flat mainstem moving down the centre of the lake account for the encircled line of negative bias points (~-1 m) at a range of different slopes in Figure 6c. The range of channel slopes for the lake are due to the transition from the steep slopes either side of Lake Malawi to the flat mainstem in the middle of the lake. Results for lakes are usually discarded and replaced by a water mask when postprocessing the GFM data,

545 meaning the impact on risk estimates from the GFM is likely to be small. However, an improved
546 consideration of lakes will be needed for the GFM to simulate lake levels. There are also some
547 cases of positive errors in the shallow water flow zone, these indicate the potential for reduced
548 accuracy under such conditions. However, the same errors are present in the Manning's method
549 used for initial conditions, which are not corrected by the simple optimisation routine used here.
550 Implementing the nonlinear least squares estimation method from test 1 or supercritical flow
551 profiles may be necessary in some location to gain accurate results.

552 Although errors in the water surface profile can be several meters greater for the Manning's
553 method than the GVF method we do not expect such large errors in water surface elevation to
554 propagate into the inundation extents because floodplain storage and conveyance will dampen
555 the wave amplitude. Figure 4 plots the flood inundation extents for the 1 in 5 year return period
556 flood to assess the impact of the surface profile errors on inundation simulation. Flood extent
557 was 40.3% greater for the Manning's method and total floodplain storage increased by 79.4%.
558 Meanwhile exposure to this return period was 150,000 people for the Manning's method and
559 90,000 people for the GVF method according to High Resolution Settlement Layer (HRSL)
560 population data (https://www.ciesin.columbia.edu/data/hrsl/). Therefore, inaccurate specification
561 of the channel bed by not accounting for nonuniform flow will bias flood inundation and
562 exposure calculations. Studies that use such methods for management activities such as assessing
563 the value of floodplains for wave attenuation and national/international scale overviews of flood
564 defence requirements (especially for low return period events) should take note of these
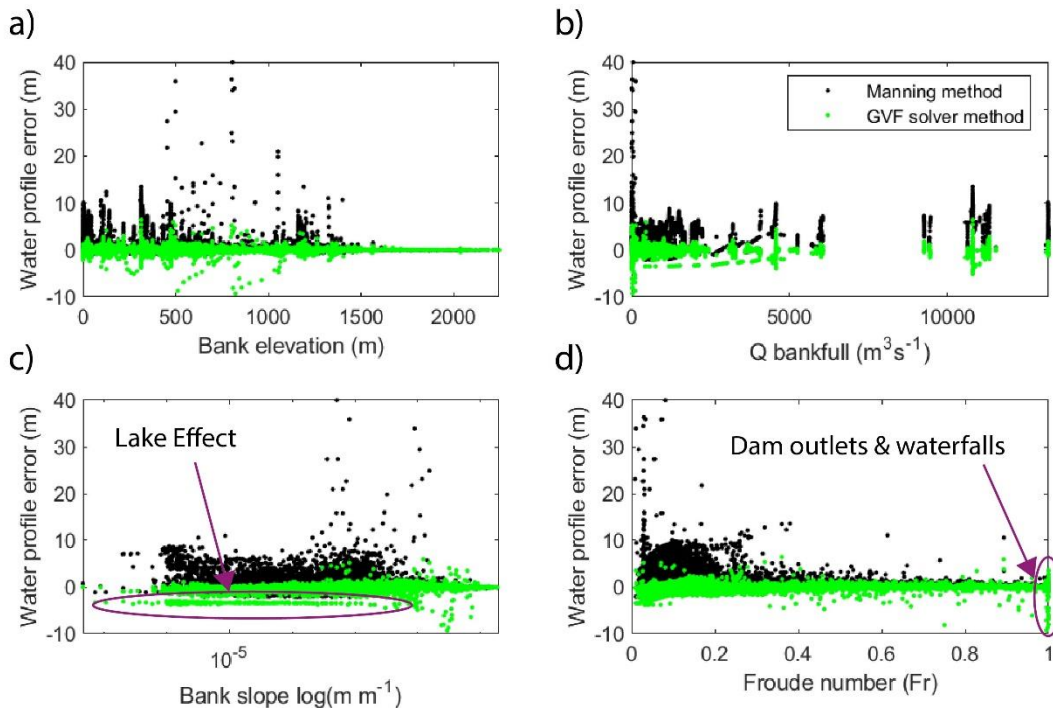565 substantial biases.

566

567 **Figure 6.** Plots of water surface profile errors against a) bank elevation, b) bankfull discharge, c)
568 logged bank slope and d) Froude number. Black dots are for the Manning's method bed
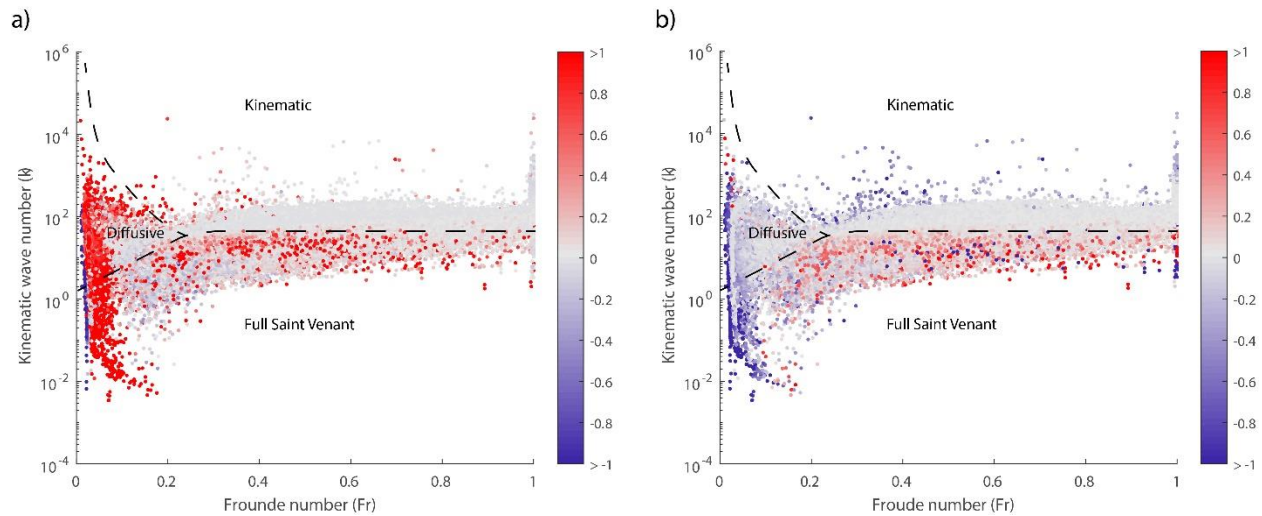569 estimated and green dots are for the GFV method.

570

Figure 7. Plots of log kinematic wave number against Froude number for every point on the river network. Colours indicate water surface profile errors (truncated at ±1 m) for a) the Manning's method and b) GVF method. Lines indicate approximate boundaries between wave types.

4 Conclusions

This paper has developed and demonstrated methods for channel bed estimation based on a simple gradually varied flow solver, which are suitable for application in reach scale and global scale flood models. The principal of considering nonuniform flow rather than uniform flow when estimating the bed elevations was first evaluated on a well-studied site in the UK where the accuracy of the approach could be assessed, and different numerical methods evaluated. We found that:

i)   The GFV method outperformed a Manning's equation method and could reconstruct a LiDAR observed water surface profile to within the expected observation errors (<10 cm RMSE).

ii) Regularization was necessary to provide realistic bed profiles. For our test, an effective way to do this was to add a cost to the objective function for stepwise changes in bed elevation scaled in proportion to the reach slope.

iii) The method was robust when given friction parameterisations within typical ranges and poor initial bed estimates.

iv) The bed estimation process also performed well across resolutions from 100 m to 2 km, although cost increased rapidly for negligible accuracy gain towards 100 m resolution and accuracy was reduced between 1 km and 2 km resolution.

A simplified GVF bed estimation method was implemented in a global flood model (Sampson et al., 2015). Results from a test case in east Africa demonstrated that water surface profile errors were reduced from 0.872 m for the Manning's method to 0.291 m for the GVF method. Bias towards over prediction by the Manning's method was also eliminated with mean error falling from 0.167 m for the Manning's model to -0.030 m for the GVF method. Improvements over the Manning's method were greatest for reaches with diffusive or shallow water wave properties, highlighting the importance of backwater effects on the flow profile.

The improved bed estimates had a substantial impact on floodplain inundation and storage dynamics for small floods when use in a hydrodynamic model. For the 1 in 5 year return period, inundation extent was reduced by 40.3%, total floodplain storage decreased by 79.4% and exposure fell from 150,000 people to 90,000 people over the study domain. Therefore, inaccurate specification of the channel bed by not accounting for nonuniform flows biased flood inundation, storage and exposure calculations. Studies that use such methods for management activities such as assessing the value of floodplains for wave attenuation and national/international scale overviews of flood defence requirements (especially for low return period events) should take note of these biases. Similarly, any flood defences added to the model will likely underperform during hydrodynamic simulation for the same reasons. For financial services applications, where catastrophe risk modelling based on event sets is often needed, the issue is particularly acute. This is because event sets must simulate flooding from both large and small return period flows in order to estimate key risk metrics such as loss exceedance probabilities. These are unlikely to be accurate with channel geometries based on Manning's equation or other simpler methods because of too much flooding for lower return period flows.

References

Adams, J. M., Gasparini, N. M., Hobley, D. E. J., Tucker, G. E., Hutton, E. W. H., Nudurupati, S. S., & Istanbulluoglu, E. (2017). The Landlab v1.0 OverlandFlow component: a Python tool for computing shallow-water flow across watersheds. *Geosci. Model Dev., 10*(4), 1645-1663. https://gmd.copernicus.org/articles/10/1645/2017/

Alfieri, L., Bisselink, B., Dottori, F., Naumann, G., de Roo, A., Salamon, P., et al. (2017). Global projections of river flood risk in a warmer world. *Earths Future, 5*(2), 171-182. <Go to ISI>://WOS:000396932200004

Alfieri, L., Salamon, P., Bianchi, A., Neal, J., Bates, P., & Feyen, L. (2014). Advances in pan-European flood hazard mapping. *Hydrological Processes, 28*(13), 4067-4077.

Allen, G. H., & Pavelsky, T. M. (2018). Global extent of rivers and streams. *Science, 361*(6402), 585-588. https://science.sciencemag.org/content/sci/361/6402/585.full.pdf

Andreadis, K. M., Clark, E. A., Lettenmaier, D. P., & Alsdorf, D. E. (2007). Prospects for river discharge and depth estimation through assimilation of swath-altimetry into a raster-based hydrodynamics model. *Geophysical Research Letters, 34*(10).

Andreadis, K. M., Schumann, G. J.-P., & Pavelsky, T. (2013). A simple global river bankfull width and depth database. *Water Resources Research, 49*(10), 7164-7168. https://agupubs.onlinelibrary.wiley.com/doi/abs/10.1002/wrcr.20440

643 Bates, P. D., Horritt, M. S., & Fewtrell, T. J. (2010). A simple inertial formulation of the shallow water
644 equations for efficient two-dimensional flood inundation modelling. *Journal of Hydrology,*
645 *387*(1-2), 33-45. <Go to ISI>://WOS:000278786900004
646 Bates, P. D., Wilson, M. D., Horritt, M. S., Mason, D. C., Holden, N., & Currie, A. (2006). Reach scale
647 floodplain inundation dynamics observed using airborne synthetic aperture radar imagery: Data
648 analysis and modelling. *Journal of Hydrology, 328*(1-2), 306-318. <Go to
649 ISI>://WOS:000240248300025
650 Bell, V. A., Kay, A. L., Jones, R. G., & Moore, R. J. (2007). Development of a high resolution grid-based
651 river flow model for use with regional climate model output. *Hydrology and Earth System*
652 *Sciences, 11*(1), 532-549. <Go to ISI>://WOS:000244861700009
653 Bernhofen, M. V., Whyman, C., Trigg, M. A., Sleigh, P. A., Smith, A. M., Sampson, C. C., et al. (2018). A
654 first collective validation of global fluvial flood models for major floods in Nigeria and
655 Mozambique. *Environmental Research Letters, 13*(10), 104007. http://dx.doi.org/10.1088/1748-
656 9326/aae014
657 Biancamaria, S., Durand, M., Andreadis, K. M., Bates, P. D., Boone, A., Mognard, N. M., et al. (2011).
658 Assimilation of virtual wide swath altimetry to improve Arctic river modeling. *Remote Sensing of*
659 *Environment, 115*(2), 373-381. <Go to ISI>://WOS:000286782500010
660 Bradbrook, K., Waller, S., & Morris, D. (2005). National Floodplain Mapping: Datasets and Methods –
661 160,000 km in 12 months. *Natural Hazards, 36*(1), 103-123. journal article.
662 https://doi.org/10.1007/s11069-004-4544-9
663 Brêda, J. P. L. F., Paiva, R. C. D., Bravo, J. M., Passaia, O. A., & Moreira, D. M. (2019). Assimilation of
664 Satellite Altimetry Data for Effective River Bathymetry. *Water Resources Research, 55*(9), 7441-
665 7463. https://agupubs.onlinelibrary.wiley.com/doi/abs/10.1029/2018WR024010
666 Chaudhry, H. M. (2008). *Open-Channel Flow*. Boston, MA: Springer.
667 Cook, A., & Merwade, V. (2009). Effect of topographic data, geometric configuration and modeling
668 approach on flood inundation mapping. *Journal of Hydrology, 377*(1-2), 131-142. <Go to
669 ISI>://WOS:000271125800014
670 Courty, L. G., Soriano-Monzalvo, J. C., & Pedrozo-Acuña, A. (2019). Evaluation of open-access global
671 digital elevation models (AW3D30, SRTM, and ASTER) for flood modelling purposes. *Journal of*
672 *Flood Risk Management, 12*(S1), e12550.
673 https://onlinelibrary.wiley.com/doi/abs/10.1111/jfr3.12550
674 Dadson, S. J., Ashpole, I., Harris, P., Davies, H. N., Clark, D. B., Blyth, E., & Taylor, C. M. (2010). Wetland
675 inundation dynamics in a model of land surface climate: Evaluation in the Niger inland delta
676 region. *Journal of Geophysical Research-Atmospheres, 115*. <Go to ISI>://000285017500008
677 de Almeida, G. A. M., Bates, P., Freer, J. E., & Souvignet, M. (2012). Improving the stability of a simple
678 formulation of the shallow water equations for 2-D flood modeling. *Water Resources Research,*
679 *48*. <Go to ISI>://WOS:000304253400004
680 de Moel, H., van Alphen, J., & Aerts, J. C. J. H. (2009). Flood maps in Europe – methods,
681 availability and use. *Nat. Hazards Earth Syst. Sci., 9*(2), 289-301. https://www.nat-hazards-earth-
682 syst-sci.net/9/289/2009/
683 Decharme, B., Douville, H., Prigent, C., Papa, F., & Aires, F. (2008). A new river flooding scheme for global
684 climate applications: Off-line evaluation over South America. *Journal of Geophysical Research-*
685 *Atmospheres, 113*(D11). <Go to ISI>://WOS:000256561000005
686 Dottori, F., Salamon, P., Bianchi, A., Alfieri, L., Hirpa, F. A., & Feyen, L. (2016). Development and
687 evaluation of a framework for global flood hazard mapping. *Advances in Water Resources, 94*,
688 87-102. <Go to ISI>://WOS:000381529000008

689   Dottori, F., Szewczyk, W., Ciscar, J. C., Zhao, F., Alfieri, L., Hirabayashi, Y., et al. (2018). Increased human
690   and economic losses from river flooding with anthropogenic warming. *Nature Climate Change,*
691   *8*(9), 781-+. <Go to ISI>://WOS:000443195300014
692   Durand, M., Andreadis, K. M., Alsdorf, D. E., Lettenmaier, D. P., Moller, D., & Wilson, M. (2008).
693   Estimation of bathymetric depth and slope from data assimilation of swath altimetry into a
694   hydrodynamic model. *Geophysical Research Letters, 35*(20).
695   Durand, M., Gleason, C. J., Garambois, P. A., Bjerklie, D., Smith, L. C., Roux, H., et al. (2016). An
696   intercomparison of remote sensing river discharge estimation algorithms from measurements of
697   river height, width, and slope. *Water Resources Research, 52*(6), 4527-4549. Article.
698   http://www.scopus.com/inward/record.url?scp=84978032829&partnerID=8YFLogxK
699   Durand, M., Neal, J., Rodriguez, E., Andreadis, K. M., Smith, L. C., & Yoon, Y. (2014). Estimating reach-
700   averaged discharge for the River Severn from measurements of river water surface elevation
701   and slope. *Journal of Hydrology, 511*, 92-104.
702   Ettritch, G., Hardy, A., Bojang, L., Cross, D., Bunting, P., & Brewer, P. (2018). Enhancing digital elevation
703   models for hydraulic modelling using flood frequency detection. *Remote Sensing of*
704   *Environment, 217*, 506-522.
705   http://www.sciencedirect.com/science/article/pii/S003442571830405X
706   Fewtrell, T. J., Neal, J. C., Bates, P. D., & Harrison, P. J. (2011). Geometric and structural river channel
707   complexity and the prediction of urban inundation. *Hydrological Processes, 25*(20), 3173-3186.
708   https://onlinelibrary.wiley.com/doi/abs/10.1002/hyp.8035
709   *Flood estimation handbook*. (1999). Wallingford: Institute of Hydrology.
710   Garambois, P. A., & Monnier, J. (2015). Inference of effective river properties from remotely sensed
711   observations of water surface. *Advances in Water Resources, 79*, 103-120. <Go to
712   ISI>://WOS:000352500000008
713   García-Pintado, J., Mason, D. C., Dance, S. L., Cloke, H. L., Neal, J. C., Freer, J., & Bates, P. D. (2015).
714   Satellite-supported flood forecasting in river networks. *Journal of Hydrology, 523*, 706-724.
715   Article. http://www.scopus.com/inward/record.url?scp=84923365791&partnerID=8YFLogxK
716   Gleason, C. J., & Smith, L. C. (2014). Toward global mapping of river discharge using satellite images and
717   at-many-stations hydraulic geometry. *Proceedings of the National Academy of Sciences, 111*(13),
718   4788-4791. https://www.pnas.org/content/pnas/111/13/4788.full.pdf
719   Grimaldi, S., Li, Y., Walker, J. P., & Pauwels, V. R. N. (2018). Effective Representation of River Geometry
720   in Hydraulic Flood Forecast Models. *Water Resources Research, 54*(2), 1031-1057.
721   https://agupubs.onlinelibrary.wiley.com/doi/abs/10.1002/2017WR021765
722   Hawker, L., Rougier, J., Neal, J., Bates, P., Archer, L., & Yamazaki, D. (2018). Implications of Simulating
723   Global Digital Elevation Models for Flood Inundation Studies. *Water Resources Research, 54*(10),
724   7910-7928. https://agupubs.onlinelibrary.wiley.com/doi/abs/10.1029/2018WR023279
725   Henderson, F. M. (1966). *Open Channel Flow*. New York: Macmillan.
726   Hey, R. D., & Thorne, C. R. (1986). STABLE CHANNELS WITH MOBILE GRAVEL BEDS. *Journal of Hydraulic*
727   *Engineering-Asce, 112*(8), 671-689. <Go to ISI>://WOS:A1986E789800002
728   Hirabayashi, Y., Mahendran, R., Koirala, S., Konoshima, L., Yamazaki, D., Watanabe, S., et al. (2013).
729   Global flood risk under climate change. *Nature Climate Change, 3*(9), 816-821.
730   https://doi.org/10.1038/nclimate1911
731   Ikeuchi, H., Hirabayashi, Y., Yamazaki, D., Kiguchi, M., Koirala, S., Nagano, T., et al. (2015). Modeling
732   complex flow dynamics of fluvial floods exacerbated by sea level rise in the Ganges–
733   Brahmaputra–Meghna Delta. *Environmental Research Letters, 10*(12), 124011.
734   http://dx.doi.org/10.1088/1748-9326/10/12/124011

735 Isikdogan, F., Bovik, A., & Passalacqua, P. (2017). RivaMap: An automated river analysis and mapping
736   engine. *Remote Sensing of Environment, 202*, 88-97.
737   http://www.sciencedirect.com/science/article/pii/S0034425717301475
738 Jongman, B., Ward, P. J., & Aerts, J. C. J. H. (2012). Global exposure to river and coastal flooding: Long
739   term trends and changes. *Global Environmental Change, 22*(4), 823-835.
740   http://www.sciencedirect.com/science/article/pii/S0959378012000830
741 Knight, D. W., & Shiono, K. (1996). River channel and floodplain hydraulics. In W. Anderson, and Bates
742   (Ed.), *Floodplain processes* (pp. 139-181). New York: Wiley.
743 Lewin, J., & Ashworth, P. J. (2014). The negative relief of large river floodplains. *Earth-Science Reviews,*
744   *129*, 1-23. http://www.sciencedirect.com/science/article/pii/S0012825213001864
745 Lin, P., Pan, M., Allen, G. H., de Frasson, R. P., Zeng, Z., Yamazaki, D., & Wood, E. F. (2020). Global
746   Estimates of Reach-Level Bankfull River Width Leveraging Big Data Geospatial Analysis.
747   *Geophysical Research Letters, 47*(7), e2019GL086405.
748   https://agupubs.onlinelibrary.wiley.com/doi/abs/10.1029/2019GL086405
749 Lohmann, D., Raschke, E., Nijssen, B., & Lettenmaier, D. P. (1998). Regional scale hydrology: I.
750   Formulation of the VIC-2L model coupled to a routing model. *Hydrological Sciences Journal,*
751   *43*(1), 131-141. http://dx.doi.org/10.1080/02626669809492107
752 Marks, K., & Bates, P. (2000). Integration of high-resolution topographic data with floodplain flow
753   models. *Hydrological Processes, 14*(11-12), 2109-2122. <Go to ISI>://WOS:000088879600014
754 Merz, B., Hall, J., Disse, M., & Schumann, A. (2010). Fluvial flood risk management in a changing world.
755   *Nat. Hazards Earth Syst. Sci., 10*(3), 509-527. https://www.nat-hazards-earth-syst-
756   sci.net/10/509/2010/
757 More, J. J., & Sorensen, D. C. (1983). Computing a Trust Region Step. *Siam Journal on Scientific and*
758   *Statistical Computing, 4*(3), 553-572. <Go to ISI>://WOS:A1983RU72300010
759 Nardi, F., Annis, A., Di Baldassarre, G., Vivoni, E. R., & Grimaldi, S. (2019). GFPLAIN250m, a global high-
760   resolution dataset of Earth's floodplains. *Scientific Data, 6*(1), 180309.
761   https://doi.org/10.1038/sdata.2018.309
762 Neal, J., Schumann, G., & Bates, P. (2012). A subgrid channel model for simulating river hydraulics and
763   floodplain inundation over large and data sparse areas. *Water Resources Research, 48*. <Go to
764   ISI>://WOS:000310961300003
765 Neal, J., Schumann, G., Bates, P., Buytaert, W., Matgen, P., & Pappenberger, F. (2009). A data
766   assimilation approach to discharge estimation from space. *Hydrological Processes, 23*(25), 3641-
767   3649.
768 Neal, J. C., Odoni, N. A., Trigg, M. A., Freer, J. E., Garcia-Pintado, J., Mason, D. C., et al. (2015). Efficient
769   incorporation of channel cross-section geometry uncertainty into regional and global scale flood
770   inundation models. *Journal of Hydrology, 529*, 169-183.
771 Oki, T., & Sud, Y. C. (1998). Design of Total Runoff Integrating Pathways (TRIP)—A Global River Channel
772   Network. *Earth Interactions, 2*(1), 1-37. http://dx.doi.org/10.1175/1087-
773   3562(1998)002<0001:DOTRIP>2.3.CO;2
774 Paiva, R. C. D., Collischonn, W., & Tucci, C. E. M. (2011). Large scale hydrologic and hydrodynamic
775   modeling using limited data and a GIS based approach. *Journal of Hydrology, 406*(3–4), 170-181.
776   http://www.sciencedirect.com/science/article/pii/S0022169411004045
777 Pappenberger, F., Dutra, E., Wetterhall, F., & Cloke, H. L. (2012). Deriving global flood hazard maps of
778   fluvial floods through a physical model cascade. *Hydrol. Earth Syst. Sci., 16*(11), 4143-4156.
779   https://www.hydrol-earth-syst-sci.net/16/4143/2012/
780 Pappenberger, F., Matgen, P., Beven, K. J., Henry, J. B., Pfister, L., & Fraipont de, P. (2006). Influence of
781   uncertain boundary conditions and model structure on flood inundation predictions. *Advances*
782   *in Water Resources, 29*(10), 1430-1449. <Go to ISI>://WOS:000241257400002

Priest, S. J., Suykens, C., Van Rijswick, H. F. M. W., Schellenberger, T., Goytia, S., Kundzewicz, Z. W., et al. (2016). The European Union approach to flood risk management and improving societal resilience

lessons from the implementation of the Floods Directive in six European countries. *Ecology and Society, 21*(4). www.jstor.org/stable/26270028

Quinn, N., Bates, P. D., Neal, J., Smith, A., Wing, O., Sampson, C., et al. (2019). The Spatial Dependence of Flood Hazard and Risk in the United States. *Water Resources Research, 55*(3), 1890-1911. <Go to ISI>://WOS:000464660000008

Sampson, C. C., Smith, A. M., Bates, P. B., Neal, J. C., Alfieri, L., & Freer, J. E. (2015). A high-resolution global flood hazard model. *Water Resources Research, 51*(9), 7358-7381. Article. http://www.scopus.com/inward/record.url?scp=84944441730&partnerID=8YFLogxK

Sanders, B. F. (2007). Evaluation of on-line DEMs for flood inundation modeling. *Advances in Water Resources, 30*(8), 1831-1843.

Sanders, B. F., & Schubert, J. E. (2019). PRIMo: Parallel raster inundation model. *Advances in Water Resources, 126*, 79-95. <Go to ISI>://WOS:000461611900007

Sanders, R., Shaw, F., MacKay, H., Galy, H., & Foote, M. (2005). National flood modelling for insurance purposes: using IFSAR for flood risk estimation in Europe. *Hydrology and Earth System Sciences, 9*(4), 449-456.

Sayama, T., Ozawa, G., Kawakami, T., Nabesaka, S., & Fukami, K. (2012). Rainfall–runoff–inundation analysis of the 2010 Pakistan flood in the Kabul River basin. *Hydrological Sciences Journal, 57*(2), 298-312. http://dx.doi.org/10.1080/02626667.2011.644245

Schumann, G.-P., Neal, J. C., Fewtrell, T. J., Bates, P. D., & Mason, D. (2009). A comprehensive space-borne SAR dataset to investigate flood processes: a case study of the England 2007 summer floods. In *Proceedings of the EO and water cycle science conference organised by ESA, EGU, ISPRS and GEWEX, 18-20 Nov 2009, Frascati, Italy*.

Scussolini, P., Aerts, J. C. J. H., Jongman, B., Bouwer, L. M., Winsemius, H. C., de Moel, H., & Ward, P. J. (2016). FLOPROS: an evolving global database of flood protection standards. *Nat. Hazards Earth Syst. Sci., 16*(5), 1049-1061. https://www.nat-hazards-earth-syst-sci.net/16/1049/2016/

Sellier, M. (2016). Inverse problems in free surface flows: a review. *Acta Mechanica, 227*(3), 913-935. journal article. https://doi.org/10.1007/s00707-015-1477-1

Smart, G. M., Bind, J., & Duncan, M. J. (2009). River bathymetry from conventional LiDAR using water surface returns. *18th World Imacs Congress and Modsim09 International Congress on Modelling and Simulation*, 2521-2527. <Go to ISI>://WOS:000290045002086

Smith, A., Sampson, C., & Bates, P. (2015). Regional flood frequency analysis at the global scale. *Water Resources Research, 51*(1), 539-553. <Go to ISI>://WOS:000349889800030

Trigg, M., Birch, C., Neal, J., Bates, P., Smith, A., Sampson, C., et al. (2016). The credibility challenge for global fluvial flood risk analysis. *Environmental Research Letters, 11*(9). Article. http://www.scopus.com/inward/record.url?scp=84992052824&partnerID=8YFLogxK

Trigg, M. A., Bates, P. D., Wilson, M. D., Schumann, G., & Baugh, C. (2012). Floodplain channel morphology and networks of the middle Amazon River. *Water Resources Research, 48*(10). https://agupubs.onlinelibrary.wiley.com/doi/abs/10.1029/2012WR011888

Trigg, M. A., Wilson, M. D., Bates, P. D., Horritt, M. S., Alsdorf, D. E., Forsberg, B. R., & Vega, M. C. (2009). Amazon flood wave hydraulics. *Journal of Hydrology, 374*(1), 92-105. http://www.sciencedirect.com/science/article/pii/S0022169409003278

UNISDR. (2015). *GAR 2015 Global Assessment Report on Disaster Risk Reduction, Making Development Sustainable: The Future of Disaster Risk Management*

Retrieved from Geneva: www.preventionweb.net/english/hyogo/gar/2015/en/gar-pdf/GAR2015_EN.pdf

831 Van Alphen, J., Martini, F., Loat, R., Slomp, R., & Passchier, R. (2009). Flood risk mapping in Europe,
832   experiences and best practices. *Journal of Flood Risk Management, 2*(4), 285-292.
833   https://onlinelibrary.wiley.com/doi/abs/10.1111/j.1753-318X.2009.01045.x
834 Vieira, J. H. D. (1983). Conditions governing the use of approximations for the Saint-Vénant equations
835   for shallow surface water flow. *Journal of Hydrology, 60*(1), 43-58.
836   http://www.sciencedirect.com/science/article/pii/0022169483900136
837 Ward, P. J., Jongman, B., Salamon, P., Simpson, A., Bates, P., De Groeve, T., et al. (2015). Usefulness and
838   limitations of global flood risk models. *Nature Climate Change, 5*(8), 712-715.
839   https://doi.org/10.1038/nclimate2742
840 Ward, P. J., Jongman, B., Weiland, F. S., Bouwman, A., van Beek, R., Bierkens, M. F. P., et al. (2013).
841   Assessing flood risk at the global scale: model setup, results, and sensitivity. *Environmental
842   Research Letters, 8*(4), 044019. http://dx.doi.org/10.1088/1748-9326/8/4/044019
843 Wing, O. E. J., Bates, P. D., Sampson, C. C., Smith, A. M., Johnson, K. A., & Erickson, T. A. (2017).
844   Validation of a 30 m resolution flood hazard model of the conterminous United States. *Water
845   Resources Research, 53*(9), 7968-7986.
846   https://agupubs.onlinelibrary.wiley.com/doi/abs/10.1002/2017WR020917
847 Winsemius, H. C., Van Beek, L. P. H., Jongman, B., Ward, P. J., & Bouwman, A. (2013). A framework for
848   global river flood risk assessments. *Hydrology and Earth System Sciences, 17*(5), 1871-1892. <Go
849   to ISI>://WOS:000319857200014
850 Yamazaki, D., de Almeida, G. A. M., & Bates, P. D. (2013). Improving computational efficiency in global
851   river models by implementing the local inertial flow equation and a vector-based river network
852   map. *Water Resources Research, 49*(11), 7221-7235.
853   https://agupubs.onlinelibrary.wiley.com/doi/abs/10.1002/wrcr.20552
854 Yamazaki, D., Ikeshima, D., Sosa, J., Bates, P. D., Allen, G. H., & Pavelsky, T. M. (2019). MERIT Hydro: A
855   High-Resolution Global Hydrography Map Based on Latest Topography Dataset. *Water
856   Resources Research, 55*(6), 5053-5073.
857   https://agupubs.onlinelibrary.wiley.com/doi/abs/10.1029/2019WR024873
858 Yamazaki, D., Ikeshima, D., Tawatari, R., Yamaguchi, T., O'Loughlin, F., Neal, J. C., et al. (2017). A high-
859   accuracy map of global terrain elevations. *Geophysical Research Letters, 44*(11), 5844-5853.
860   Article. http://www.scopus.com/inward/record.url?scp=85020717905&partnerID=8YFLogxK
861 Yamazaki, D., Kanae, S., Kim, H., & Oki, T. (2011). A physically based description of floodplain inundation
862   dynamics in a global river routing model. *Water Resources Research, 47*. <Go to
863   ISI>://WOS:000289087600001
864 Yang, X., Pavelsky, T. M., Allen, G. H., & Donchyts, G. (2020). RivWidthCloud: An Automated Google
865   Earth Engine Algorithm for River Width Extraction From Remotely Sensed Imagery. *Ieee
866   Geoscience and Remote Sensing Letters, 17*(2), 217-221.
867